Semicond. Sci. Technol. **23** (2008) 114003 (11pp) doi:10.1088/0268-1242/23/11/114003

Magneto-gyrotropic effects in semiconductor quantum wells

V V Bel'kov[1,2] **and S D Ganichev**[1]

[1] Terahertz Center, University of Regensburg, 93040 Regensburg, Germany
[2] A F Ioffe Physico-Technical Institute, Russian Academy of Sciences, 194021 St Petersburg, Russia

E-mail: sergey.ganichev@physik.uni-regensburg.de

Received 3 March 2008
Published 29 October 2008
Online at stacks.iop.org/SST/23/114003

Abstract
Magneto-gyrotropic photogalvanic effects in quantum wells are reviewed. We discuss experimental data, results of phenomenological analysis and microscopic models of these effects. The current flow is driven by spin-dependent scattering in low-dimensional structure gyrotropic media resulting in asymmetry of photoexcitation and relaxation processes. Several applications of the effects are also considered.

(Some figures in this article are in colour only in the electronic version)

1. Introduction

The spin of electrons and holes in solid state systems is an intensively studied quantum mechanical property showing a large variety of interesting physical phenomena. One of the most frequently used and powerful methods of generation and investigation of spin polarization is optical orientation [1]. Besides purely optical phenomena, like circularly polarized photoluminescence, the optical generation of an unbalanced spin distribution in a semiconductor may lead to spin photocurrents. Light propagating through a semiconductor and acting upon mobile carriers can generate a dc electric current, under short-circuit condition, or a voltage, in the case of open-circuit samples. A spin photocurrent was proposed for the first time in [2] (see also [3]) and thereafter observed in bulk AlGaAs [4]. In these works, it has been shown that an inhomogeneity of the spin-polarized electrons results in a surface current due to spin–orbit interaction. A gradient of spin density was obtained by making use of the strong fundamental absorption of circularly polarized light at the band edge of the bulk semiconductor. Recent studies [5] demonstrated that spin photocurrents can also be generated by homogeneous spin polarization caused by absorption of circularly polarized radiation in low-dimensional systems, such as circular photogalvanic effect or spin-galvanic effect (SGE), or even as a result of the illumination with unpolarized radiation due to magneto-gyrotropic photogalvanic effects (MGE). All these phenomena are gathered in the class of photogalvanic effects (PGE), which, by definition, appear neither due to inhomogeneity of optical excitation of electron–hole pairs nor due to inhomogeneity of the sample.

In this paper, we consider only the magnetic-field-induced photogalvanic effects in low-dimensional semiconductor structures. Moreover, we focus the attention here on the spin-photogalvanics and discuss spin-related mechanisms of magneto-gyrotropic photogalvanic effects due to the Larmor-precession-induced spin-galvanic effect and caused by zero-bias spin separation. Microscopic mechanisms of these phenomena are given in section 2. They are based on the spin–orbit coupling which provides a versatile tool to generate and to manipulate the spin degree of freedom in low-dimensional semiconductor structures. In general, the zero-bias spin separation and spin-galvanic effect do not require an application of an external magnetic effect and for some mechanisms even light. However, they have been demonstrated and are most intensively studied applying the MGE technique. The macroscopic features of all magneto-gyrotropic effects discussed here, e.g., the possibility of generating a photocurrent, its behavior upon variation of radiation polarization, crystallographic orientation, experimental geometry, etc, are described in the frame of a phenomenological theory presented in section 3. Phenomenological theory operates with conventional vectors, or *polar* vectors, and pseudo-vectors, or *axial* vectors, and indeed does not depend on details of microscopic mechanisms. Section 4 gives a short account of the experimental technique. In section 5, the experimental results are presented and discussed in view of the theoretical background. In this section

 © 2008 IOP Publishing Ltd Printed in the UK

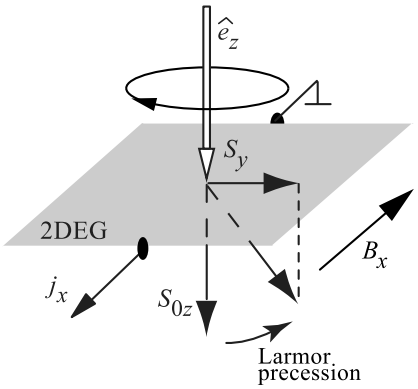

Figure 1. Optical scheme of generating a uniform in-plane spin polarization driving a spin-galvanic current. Electron spins are oriented normal to the QW plane by circularly polarized radiation and rotated into the plane by the Larmor precession in an in-plane magnetic field B_x (after [7]).

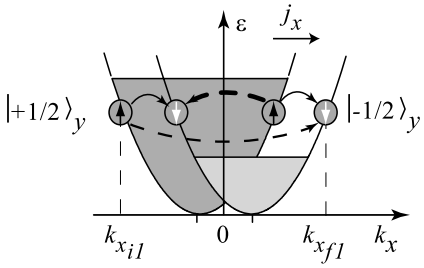

Figure 2. Microscopic origin of the spin-galvanic current in the presence of $\boldsymbol{k}$-linear terms in the electron Hamiltonian: the $\sigma_y k_x$ term in the Hamiltonian splits the conduction band into two parabolas with the spin $s = \pm 1/2$ pointing in the y-direction. If one spin subband is preferentially occupied, e.g., by spin injection (the $|+1/2\rangle_y$-states in the figure) asymmetric spin-flip scattering results in a current in the x-direction. The rate of spin-flip scattering depends on the value of the initial and final $\boldsymbol{k}$-vectors. Thus, the transitions sketched by broken arrows yield an asymmetric occupation of both subbands and hence a current flow (after [7]).

we also discuss applications of MGE; in particular, we analyze spin splitting of subbands in $\boldsymbol{k}$-space due to bulk inversion asymmetry (BIA) and structural inversion asymmetry (SIA) in QWs of various crystallographic orientations.

2. Microscopic models

2.1. Spin-galvanic effect

In a system of free carriers with nonequilibrium spin-state occupation but equilibrium energy distribution within each spin branch, the spin relaxation can result in the generation of an electric current [6]. This effect is called the spin-galvanic effect [7]. Phenomenologically, an electric current can be linked to the electron's averaged spin polarization $\boldsymbol{S}$ by

$$j_\alpha = \sum_\gamma Q_{\alpha\gamma} S_\gamma. \tag{1}$$

For (0 0 1)-grown zinc-blende structure based QWs of C_{2v}-symmetry this equation reduces to $j_x = Q_{xy} S_y$ and $j_y = Q_{yx} S_x$. Here, we choose the coordinate system as $x \parallel [1\,\bar{1}\,0]$, $y \parallel [1\,1\,0]$ and $z \parallel [0\,0\,1]$.

The spin-galvanic effect generally does not require optical excitation; in fact, the nonequilibrium spin can be achieved both by optical and non-optical methods, e.g., by electrical spin injection. If the nonequilibrium spin, however, is produced by optical orientation proportional to the degree of light circular polarization, $P_{\rm circ}$, the current generation can be regarded as a photogalvanic effect. Under pure optical excitation, the spin-galvanic effect is usually observed simultaneously with the circular photogalvanic effect. For this condition, two effects can be experimentally separated in time-resolved experiments or by spectral measurements. However, another method, which, on the one hand, provides a nonequal population of spin subbands and, on the other hand, excludes the circular PGE was proposed in [7].

The method is based on the use of optical orientation at normal incidence and the assistance of an external magnetic field to achieve an in-plane polarization in (0 0 1)-grown low-dimensional structures (see figure 1). For normal incidence the spin-galvanic effect as well as the circular PGE vanish. Thus, the spin polarization S_{0z} along the z-axis is achieved but no spin-induced photocurrent is generated[3]. An in-plane spin component, necessary for the spin-galvanic effect, arises in an in-plane magnetic field. The field perpendicular to the initially oriented spins (e.g., $\boldsymbol{B} \parallel x$) rotates them into the plane of the two-dimensional electron gas (2DEG) due to the Larmor precession (Hanle effect). The nonequilibrium spin polarization S_y is given by

$$S_y = -\frac{\omega_L \tau_{s\perp}}{1 + (\omega_L \tau_s)^2} S_{0z}, \tag{2}$$

where $\tau_s = \sqrt{\tau_{s\parallel}\tau_{s\perp}}$, $\tau_{s\parallel}$ and $\tau_{s\perp}$ are the longitudinal and transverse electron spin relaxation times, and ω_L is the Larmor frequency. The spin-galvanic effect investigated in such a geometry belongs to the class of magneto-gyrotropic effects. A characteristic feature of the magneto-gyrotropic effect due to the spin-galvanic effect is that the current reverses its direction upon changing the radiation helicity from left-handed to right-handed and vice versa as well as upon reversing the in-plane magnetic field direction. This follows from equation (1) showing that the current direction is given by the direction of the in-plane nonequilibrium spin which changes upon reversing radiation helicity or the magnetic field.

Microscopically, the spin-galvanic effect is caused by asymmetric spin-flip relaxation of spin-polarized electrons [7] in systems with $\boldsymbol{k}$-linear contributions to the effective Hamiltonian $\mathcal{H}_k = \sum_{lm} \beta_{lm} \sigma_l k_m$, where $\boldsymbol{k}$ is the electron wave vector, σ_l are the Pauli spin matrices and β_{lm} are real coefficients. The coefficients β_{lm} form a pseudo-tensor subject to the same symmetry restriction as the transposed pseudo-tensor $\boldsymbol{Q}$. The sources of Dresselhaus and Rashba

[3] We note that a similar method has been applied in the experiments of Bakun *et al* [4] carried out on bulk AlGaAs excited by inter-band absorption and demonstrating spin photocurrents caused by the inhomogeneous spin distribution predicted in [2, 3]. The crucial difference to the spin-galvanic effect is that in the case of surface photocurrent caused by optical orientation a gradient of spin density is needed. Naturally, this gradient is absent in QWs where the spin-galvanic effect has been investigated because QWs are two-dimensional and have no 'thickness'.

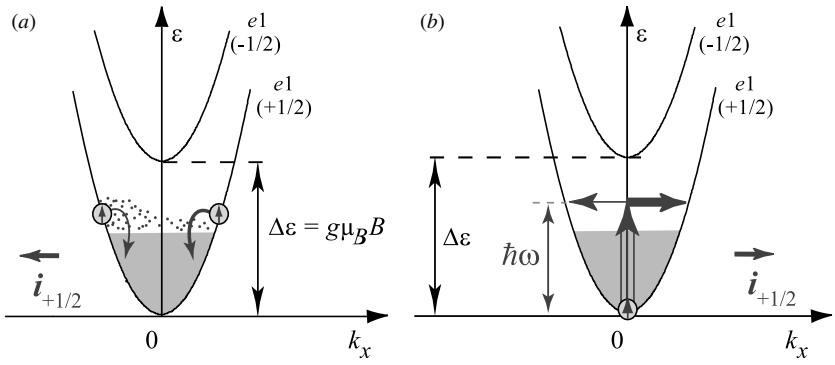

Figure 3. Microscopic origin of a zero-bias spin separation and the corresponding magnetic-field-induced photocurrent. Zero-bias spin separation is due to scattering matrix elements linear in $\boldsymbol{k}$ and σ causing asymmetric scattering and it results in spin flows. This process is sketched for the spin-up subband only and for (*a*) energy relaxation and (*b*) excitation via indirect transitions (Drude-like absorption). Here, scattering is assumed to have a larger probability for positive k_x than that for negative k_x as indicated by arrows of different thickness. Therefore, in (*a*) the energy relaxation rates for positive k_x are larger than for negative k_x and in (*b*) the rates of optical transitions for opposite wave vectors are different. This imbalance leads to a net spin-up electron flow. In the spin-down subband, the picture is mirror symmetric, resulting in a net spin-down electron flow of opposite direction. Thus, at zero magnetic field a pure spin current is generated. The corresponding electric currents have equal magnitudes and therefore cancel each other. An in-plane magnetic field, however, lifts the compensation of the oppositely directed electron flows yielding a charge current (after [12]).

$\boldsymbol{k}$-linear terms are the bulk inversion asymmetry [8] and a structural inversion asymmetry [9], respectively. For a 2DEG system, these terms lead to the situation sketched in figure 2. To be specific, we show the energy spectrum along k_x with the spin-dependent term $\beta_{yx}\sigma_y k_x$ of (0 0 1)-grown zinc-blende structure based QWs of C_{2v}-symmetry and describe the corresponding current $j_x = Q_{xy}S_y$.

Spin orientation in the y-direction causes the unbalanced population in the subbands. The current flow is caused by $\boldsymbol{k}$-dependent spin-flip relaxation processes. Spins oriented in the y-direction are scattered along k_x from the higher filled, e.g., spin-up subband, $|+1/2\rangle_y$, to the less filled spin-down subband, $|-1/2\rangle_y$. Four quantitatively different spin-flip scattering events exist and are sketched in figure 2 by bent arrows. The spin-flip scattering rate depends on the values of the wave vectors of the initial and final states [10]. Two scattering processes shown by broken arrows are inequivalent and generate an asymmetric carrier distribution around the subband minima in both subbands. This asymmetric population results in a current flow along the x-direction. The uniformity of spin polarization in space is preserved during the scattering processes.

2.2. Zero-bias spin separation and magneto-gyrotropic effects

For linearly polarized radiation the magneto-gyrotropic effect due to the spin-galvanic effect vanishes because the light absorption does not result in nonequilibrium spin. However, in an external magnetic field other kinds of spin photocurrents may be generated even by unpolarized radiation as has been proposed for bulk gyrotropic crystals [11]. The microscopic mechanisms of this type of spin photocurrents in low-dimensional structures have been developed most recently to describe terahertz (THz) radiation induced photocurrents observed in GaAs-, InAs-, SiGe- and GaN-based structures [5]. It has been shown that the free-carrier absorption of THz radiation results in a pure spin current and the corresponding spin separation achieved by spin-dependent scattering of electrons in gyrotropic media. The pure spin current in these experiments is converted into an electric current by an application of a magnetic field which polarizes spins due to the Zeeman effect yielding magneto-gyrotropic effects.

Spin separation due to spin-dependent scattering in gyrotropic media can be achieved in various ways but all of them must drive the electron gas into a nonequilibrium state. One straightforward method used here is to heat the electron system by THz or microwave radiation. Figure 3(*a*) sketches the process of energy relaxation of hot electrons for the spin-up subband ($s = +1/2$) in a quantum well containing a two-dimensional electron gas. Energy relaxation processes are shown by curved arrows. Usually, energy relaxation via scattering of electrons is considered to be spin independent. In gyrotropic media, like low-dimensional GaAs structures or asymmetric SiGe QWs, however, the spin–orbit interaction adds an asymmetric spin-dependent term to the scattering probability [12]. This term in the scattering matrix element is proportional to components of $[\boldsymbol{\sigma} \times (\boldsymbol{k} + \boldsymbol{k}')]$, where $\boldsymbol{\sigma}$ is the vector composed of the Pauli matrices, $\boldsymbol{k}$ and $\boldsymbol{k}'$ are the initial and scattered electron wave vectors. Due to spin-dependent scattering, transitions to positive and negative k'_x-states occur with different probabilities. Therefore, hot electrons with opposite k_x have different relaxation rates in the two spin subbands. In figure 3(*a*), this difference is indicated by arrows of different thickness. This asymmetry causes an imbalance in the distribution of carriers in both subbands ($s = \pm 1/2$) between positive and negative k_x-states. This in turn yields a net electron flow, $\boldsymbol{i}_{\pm 1/2}$, within each spin subband [12]. Since the asymmetric part of the scattering amplitude depends on spin orientation, the probabilities for scattering to positive or negative k'_x-states are inverted for spin-down and spin-up subbands. Thus, the charge currents, $\boldsymbol{j}_+ = e\boldsymbol{i}_{+1/2}$ and $\boldsymbol{j}_- = e\boldsymbol{i}_{-1/2}$, where e is the electron charge, have opposite directions because $\boldsymbol{i}_{+1/2} = -\boldsymbol{i}_{-1/2}$ and therefore

they cancel each other. Nevertheless, a finite pure spin current $\boldsymbol{J}_{\rm spin} = \frac{1}{2}(\boldsymbol{i}_{+1/2} - \boldsymbol{i}_{-1/2})$ is generated since electrons with spin-up and spin-down move in opposite directions. This leads to a spatial spin separation and spin accumulation at the edges of the sample[4].

As addressed above, pure spin current and zero-bias spin separation can be converted into a measurable electric current by an application of a magnetic field, resulting in the magneto-gyrotropic effects. Indeed, in a Zeeman spin-polarized system, the two fluxes $\boldsymbol{i}_{\pm1/2}$, whose magnitudes depend on the free-carrier densities in spin-up and spin-down subbands, $n_{\pm1/2}$, respectively, no longer compensate each other and hence yield a net electric current (see figure 3). For the case where the fluxes $\boldsymbol{i}_{\pm1/2}$ are proportional to the carrier densities $n_{\pm1/2}$, the charge current is given by

$$\boldsymbol{j} = e(\boldsymbol{i}_{+1/2} + \boldsymbol{i}_{-1/2}) = 4eS\boldsymbol{J}_{\rm spin}, \tag{3}$$

where $S = \frac{1}{2}(n_{+1/2} - n_{-1/2})/(n_{+1/2} + n_{-1/2})$ is the magnitude of the average spin. An external magnetic field $\boldsymbol{B}$ results in different populations of the two spin subbands due to the Zeeman effect. In equilibrium, the average spin is given by

$$\boldsymbol{S} = -\frac{g\mu_B \boldsymbol{B}}{4\bar{\varepsilon}}. \tag{4}$$

Here g is the electron effective g-factor, μ_B is the Bohr magneton, $\bar{\varepsilon}$ is the characteristic electron energy being equal to the Fermi energy ε_F, or to the thermal energy k_BT, for a degenerate or a non-degenerate 2DEG, respectively [12].

Similarly to the relaxation mechanism, optical excitation of free carriers by Drude absorption, also involving electron scattering, is asymmetric and yields spin separation [12]. Drude absorption is caused by indirect intraband optical transitions and includes a momentum transfer from phonons or impurities to electrons to satisfy momentum conservation. Figure 3(*b*) sketches the process of Drude absorption via virtual states for the spin-up subband. The vertical arrow indicates optical transitions from the initial state $k = 0$ while the horizontal arrows describe an elastic scattering event to a final state with either positive or negative electron wave vector. Due to the spin dependence of scattering, transitions to positive and negative k-states occur with different probabilities. This is indicated by horizontal arrows of different thicknesses. The asymmetry causes an imbalance in the distribution of photoexcited carriers in the subband between positive and negative k-states. This in turn yields electron flow. Like for the relaxation mechanism described above probabilities of scattering to positive or negative k are inverted for spin-down and spin-up subbands, spin separation takes place and applying a magnetic field results in a net electric current.

[4] In the above analysis, we do not consider the effect of a $\boldsymbol{k}$-linear spin splitting of the electron subband since it does not lead to a significant contribution to the pure spin current. In fact, to first order in spin–orbit interaction, the spin splitting of the subband results only in a relative displacement of the spin-up and spin-down branches in $\boldsymbol{k}$-space. This shift does not disturb the symmetric distribution of carriers within each subband even if the system is driven into a non-equilibrium state, e.g. by absorption of linearly polarized radiation. Hence spin splitting in $\boldsymbol{k}$-space has no essential effect on the mechanism of spin separation discussed here and can affect it only in high-order approximations

3. Phenomenological theory

Phenomenological theory of magneto-gyrotropic effects describes dependences of the photocurrent magnitude and direction on the radiation polarization state and the orientation of the magnetic field with respect to the crystallographic axes. Within the linear approximation in the magnetic field strength $\boldsymbol{B}$, magneto-gyrotropic effects are given by

$$j_\alpha = \sum_{\beta\gamma\delta} \phi_{\alpha\beta\gamma\delta} B_\beta \{E_\gamma E_\delta^\star\} + \sum_{\beta\gamma} \mu_{\alpha\beta\gamma} B_\beta \hat{e}_\gamma E_0^2 P_{\rm circ}. \tag{5}$$

Here the fourth rank pseudo-tensor ϕ is symmetric in the last two indices, E_γ are components of the complex amplitude of the radiation electric field $\boldsymbol{E}$. In the following, the field is presented as $E = E_0 e$ with E_0 being the modulus $|\boldsymbol{E}|$ and $\boldsymbol{e}$ indicating the (complex) polarization unit vector, $|e| = 1$. The symbol $\{E_\gamma E_\delta^\star\}$ means the symmetrized product of the electric field with its complex conjugate,

$$\{E_\gamma E_\delta^\star\} = \tfrac{1}{2}\left(E_\gamma E_\delta^\star + E_\delta E_\gamma^\star\right). \tag{6}$$

In the second term on the right-hand side of equation (5) $\boldsymbol{\mu}$ is a regular third rank tensor, $P_{\rm circ}$ is the helicity of the radiation and $\hat{e}$ is the unit vector pointing in the direction of light propagation. While the second term in equation (5) requires circularly polarized radiation and represents the spin-galvanic effect, the first term may be non-zero even for unpolarized radiation.

For (0 0 1)-oriented asymmetric QWs based on zinc-blende lattice III–V compounds and belonging to C_{2v} point group, the phenomenological equation (5) for the magneto-photogalvanic effects induced by normally-incident radiation reduces to [13]

$$\begin{aligned} j_x &= S_1 B_y I + S_2 B_y (|e_x|^2 - |e_y|^2) I \\ &\quad + S_3 B_x \left(e_x e_y^* + e_y e_x^*\right) I + S_4 B_x I P_{\rm circ}, \\ j_y &= S_1' B_x I + S_2' B_x (|e_x|^2 - |e_y|^2) I \\ &\quad + S_3' B_y \left(e_x e_y^* + e_y e_x^*\right) I + S_4' B_y I P_{\rm circ}, \end{aligned} \tag{7}$$

where, for simplicity, we set for the intensity $I = E_0^2$. Here, the parameters S_1 to S_4' correspond to the non-zero components of the tensors ϕ and $\boldsymbol{\mu}$ allowed by the C_{2v} point group and only in-plane components of the magnetic field are taken into account.

For linearly polarized radiation at normal incidence and $\boldsymbol{B} \parallel y$ we have

$$j_x = S_1 B_y I + S_2 B_y I \cos 2\alpha, \qquad j_y = S_3' B_y I \sin 2\alpha, \tag{8}$$

where α is the angle between the radiation polarization vector $\boldsymbol{e}$ and the y-axis.

If in experiments elliptically polarized radiation is used the spin-galvanic effect described by the last terms in equations (7) can also be non-zero. A convenient way of variation of polarization state is passing laser radiation, initially linearly polarized along the x-axis, through a $\lambda/4$-plate. Rotation of the plate by an angle φ changes helicity and the azimuth angle of the ellipse. The helicity $P_{\rm circ}$ of the incident light varies from -1 (left handed, σ_-) to $+1$ (right handed, σ_+) according to $P_{\rm circ} = \sin 2\varphi$ and the degree of linear polarization $P_{\rm lin} =$

$\sin 4\varphi/4$. The total current for normal incidence and $\boldsymbol{B} \parallel y$ is described in this case by

$$j_x = S_1 B_y I + S_2 B_y I (1 + \cos 4\varphi)/2,$$
$$j_y = S_3' B_y I \sin 4\varphi/2 + S_4' B_y I \sin 2\varphi. \quad (9)$$

It is seen that all four contributions are characterized by different dependences of the photocurrent magnitude and direction on the radiation polarization state and the orientation of the magnetic field with respect to the crystallographic axes. As a consequence, a proper choice of experimental geometry allows one to investigate each partial photocurrent separately.

4. Methods

For optical excitation mid-infrared, terahertz and visible laser radiation was used. Most of the measurements were carried out in the infrared with photon energies less than the energy gap of investigated semiconductors. For investigations of spin photocurrents infrared excitation has several advantages. First of all below the energy gap the absorption is very weak and therefore allows homogeneous excitation with marginal heating of the 2DEG. Furthermore, in contrast to inter-band excitation, there are no spurious photocurrents due to other mechanisms such as the Dember effect, photovoltaic effects at contacts and Schottky barriers, etc. Depending on the photon energy and QW band structure, mid-infrared and THz radiation induce direct optical transitions between size quantized subbands or, at longer wavelength, indirect optical transitions (Drude absorption) in the lowest subband.

A high power pulsed mid-infrared transversely excited atmospheric pressure carbon dioxide (TEA-CO_2) laser and a molecular terahertz laser [5] have been used as radiation sources in the spectral range between 9.2 μm and 496 μm with power $P \simeq 5$ kW. The corresponding photon energies $\hbar\omega$ lie in the range of 135–2 meV.

Optically pumped molecular lasers emit linearly polarized radiation whose orientation is determined by the polarization of the pump radiation. In experiment, the plane of polarization on the sample is rotated applying $\lambda/2$-plates which enable one to vary the azimuth angle α between 0° and 180° corresponding to all possible orientations of the electric field vector in the (xy)-plane. Here $\alpha = 0$ is chosen so that the radiation polarization vector on the sample is directed along the y-axis.

To investigate magneto-gyrotropic effects due to the spin-galvanic effect an elliptically, in particular circularly, polarized light is required. The polarization of the laser beam in this case is modified from linear to elliptical applying crystal quartz $\lambda/4$-plates. Usually $\varphi = 0$ is chosen for the optical axis of the quarter-wave plate coinciding with the incoming laser polarization vector.

Magneto-gyrotropic photogalvanic effects have been investigated on a large variety of low-dimensional structures comprising GaAs-, InAs-, SiGe- and GaN-based heterostructures. As follows from equation (5) the relative direction between the current and the magnetic field and polarization dependences of various current contribution can be different for various symmetry point groups. Most frequently investigations have been carried out on structures described by two point groups: C_{2v} and C_s. Higher symmetric structures (C_{2v}) were (0 0 1)-oriented asymmetric QWs and (1 1 0)-grown symmetric GaAs QWs. Structures belonging to lower symmetry class C_s were (1 1 0)-oriented asymmetric GaAs QWs. Besides these structures magneto-gyrotropic effects were observed in (0 0 1)-grown SiGe QWs of C_{2v} point group and (0 0 0 1)-grown GaN/AlGaN heterojunctions belonging to C_{3v}-symmetry. MGE has been investigated at room temperature or mounted in an optical cryostat which allowed the variation of temperature in the range of 4.2–293 K. The photocurrent j was measured in the unbiased structures via the voltage drop across a 50 Ω load resistor in a closed circuit configuration (see the inset in figure 4). An external magnetic field for room temperature is obtained by a conventional electromagnet with the magnetic field up to 1 T and at 4.2 K using a superconducting split-coil magnet with B up to 3 T.

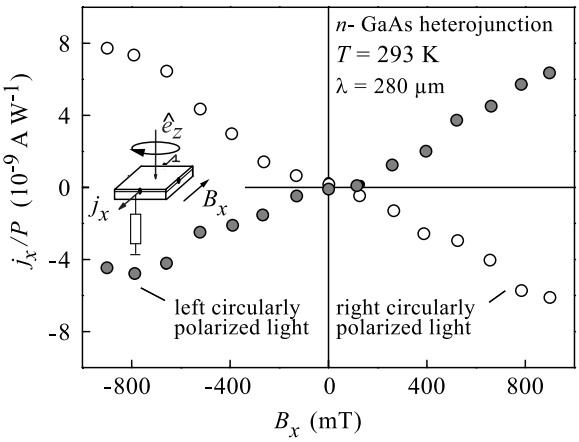

Figure 4. Magnetic field dependence of the spin-galvanic current normalized by P achieved by intra-subband transitions within $e1$ conduction subband by excitation with radiation of $\lambda = 280$ μm wavelength. Results are plotted for an (0 0 1)-grown GaAs/AlGaAs single heterojunction at room temperature (after [16]).

5. Experimental results and discussion

5.1. Magneto-gyrotropic effect due to the Larmor-precession-induced spin-galvanic photocurrent

Magneto-gyrotropic effect due to the Larmor-precession-induced spin-galvanic photocurrent has been observed for (0 0 1)-grown n-type GaAs and InAs QWs as well as for (0 0 0 1)-grown GaN/AlGaN structures applying both visible and THz radiation [7, 14]. This effect has been described in detail in several recent reviews [5, 15, 16] and we will address here only the main features of this phenomenon and discuss its application to the investigation of inversion asymmetry in quantum well structures.

Most of the experiments have been carried out applying the experimental geometry described in section 4 and sketched in figure 1. The magneto-gyrotropic effect due to the spin-galvanic effect manifests itself by the presence of the current contribution $j \propto B P_{\mathrm{circ}}$, which reverses its direction upon

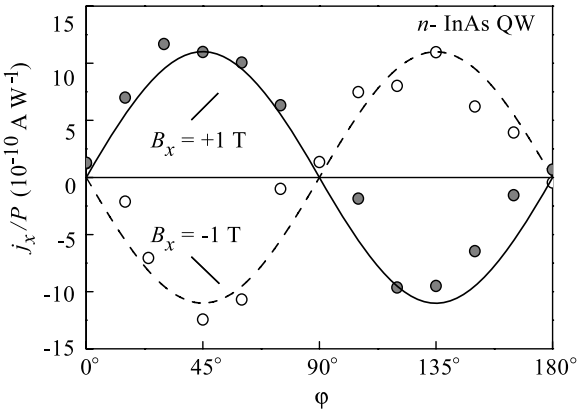

Figure 5. Spin-galvanic current normalized by P as a function of the phase angle φ in a (0 0 1)-grown n-type InAs QW of 15 nm width at $T = 4.2$ K. The photocurrent excited by normal incident radiation of $\lambda = 148$ μm is measured in the x-direction parallel (full circles) and anti-parallel (open circles) to the in-plane magnetic field B_x. Solid and dashed curves are fitted to $j_x \propto \pm \sin 2\varphi$ (after [17]).

both switching the radiation handedness for a fixed magnetic field and changing the in-plane magnetic field direction at fixed radiation helicity. Typical helicity dependence for two directions of magnetic fields is shown in figure 5. For low magnetic fields B, where $\omega_L \tau_s < 1$ holds, the current increases linearly as expected from equations (1) and (2). This is seen in the room temperature data of figure 4. The polarity of the current depends on the direction of the excited spins (S aligned along the $\pm z$-direction for right or left circularly polarized light, respectively) and on the direction of the applied magnetic field ($\pm B_x$-direction) which determines the Larmor precession direction (see figures 4 and 5). For the magnetic field applied along $\langle 1\,1\,0\rangle$, as shown in these figures, the spin-galvanic current is parallel (anti-parallel) to the magnetic field vector. For $\boldsymbol{B} \parallel \langle 1\,0\,0\rangle$, both the transverse and the longitudinal effects are observed [16].

In some experiments, carried out at low temperature and for higher magnetic fields, it is observed that with rising magnetic field strength the current assumes a maximum and decreases upon further increase of B [7]. This drop of the current is ascribed to the Hanle effect [1]. The experimental data are well described by equation (2). The observation of the Hanle effect demonstrates that free-carrier intra-subband transitions can polarize the spins of electron systems. The measurements allow one to obtain the spin relaxation time τ_s from the peak position of the photocurrent where $\omega_L \tau_s = 1$ holds [7].

We note that the observation of the mid-infrared and terahertz radiation excited spin-galvanic effect, which is due to spin orientation, gives clear evidence that direct intersubband and Drude absorption of circularly polarized radiation result in a monopolar spin orientation. Mechanisms of the monopolar spin orientation were analyzed in [18, 19].

The microscopic theory of the SGE in QWs was developed in [14, 20]. Within the model of elastic scattering the current is not spin polarized since the same number of spin-up and spin-down electrons move in the same direction with the same velocity. The spin-galvanic current can be estimated by [14]

$$j_x = Q_{xy} S_y \sim e n_s \frac{\beta_{yx}}{\hbar} \frac{\tau_p}{\tau_s'} S_y, \tag{10}$$

and a similar equation for j_y, where n_s is the 2DEG density, τ_s' is the spin relaxation time due to the Elliott–Yafet mechanism [1]. Since spin-flip scattering is the origin of the current given by equation (10), this equation is valid even if the D'yakonov–Perel' mechanism [1, 21] of spin relaxation dominates. The Elliott–Yafet relaxation time τ_s' is proportional to the momentum relaxation time τ_p. Therefore, the ratio τ_p/τ_s' in equation (10) does not depend on the momentum relaxation time. The in-plane average spin, e.g., S_y in equation (10), decays with the total spin relaxation time τ_s and, hence, the time decay of the spin-galvanic current following pulsed photoexcitation is described by the exponential function $\exp(-t/\tau_s)$. In contrast, the circular PGE current induced by a short pulse decays within the momentum relaxation time τ_p allowing us to distinguish these two effects in time-resolved measurements. In general, in addition to the kinetic contribution to the current there exists the so-called relaxational contribution which arises due to the $\boldsymbol{k}$-linear terms neglecting the Elliott–Yafet spin relaxation, i.e., with allowance for the D'yakonov–Perel' mechanism only [22].

An important application of the spin-galvanic effect is addressed in [23]. It is demonstrated that angular-dependent measurements of spin photocurrents allow one to separate the Dresselhaus and Rashba terms. These experiments were carried out on (0 0 1)-oriented QWs for which the linear in wave vector part of the Hamiltonian for the first subband reduces to

$$\mathcal{H}_{\boldsymbol{k}}^{(1)} = \alpha(\sigma_{x_0} k_{y_0} - \sigma_{y_0} k_{x_0}) + \beta(\sigma_{x_0} k_{x_0} - \sigma_{y_0} k_{y_0}), \tag{11}$$

where the parameters α and β result from the structure-inversion and bulk-inversion asymmetries, respectively, and x_0, y_0 are the crystallographic axes [1 0 0] and [0 1 0]. Note that, in the coordinate system with $x \parallel [1\,\bar{1}\,0]$ and $y \parallel [1\,1\,0]$, the matrix $\mathcal{H}_{\boldsymbol{k}}^{(1)}$ gets the form $\beta_{xy}\sigma_x k_y + \beta_{yx}\sigma_y k_x$ with $\beta_{xy} = \beta + \alpha$, $\beta_{yx} = \beta - \alpha$. According to equation (10) the current components j_x, j_y are proportional, respectively, to β_{xy} and β_{yx} and, therefore, angular-dependent measurements of spin photocurrents allow one to separate the Dresselhaus and Rashba terms. By mapping the magnitude of the spin photocurrent in the QW plane the ratio of both terms can be directly determined from experiment and does not rely on theoretically obtained quantities. The relation between the photocurrent and spin directions can be conveniently expressed in the following matrix form:

$$\boldsymbol{j} \propto \begin{pmatrix} \beta & -\alpha \\ \alpha & -\beta \end{pmatrix} \boldsymbol{S}_\parallel, \tag{12}$$

where $\boldsymbol{j}$ and $\boldsymbol{S}_\parallel$ are two-component columns with the in-plane components along the crystallographic axes $x_0 \parallel [1\,0\,0]$ and $y_0 \parallel [0\,1\,0]$. The directions of the Dresselhaus and Rashba coupling induced photocurrents are shown in figure 6(b) for the particular case $\boldsymbol{S}_\parallel \parallel [1\,0\,0]$.

Figure 6(c) shows the angular dependence of the spin-galvanic current $j(\vartheta)$ measured on n-type (0 0 1)-grown

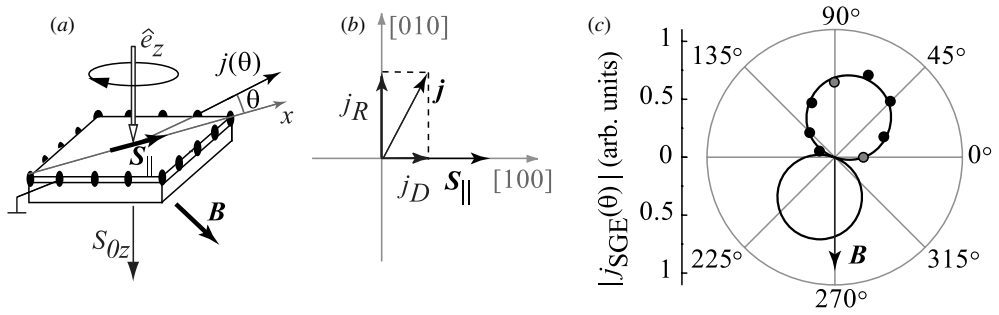

Figure 6. The separation of the Dresselhaus and Rashba contributions to the spin-galvanic effect observed in an n-type InAs single QW at room temperature for the case of the electron spin $\boldsymbol{S}_\parallel \parallel [1\,0\,0]$. (*a*) Geometry of the experiment. (*b*) The direction of Dresselhaus and Rashba contributions to the photocurrent. (*c*) The spin-galvanic current measured as a function of the angle ϑ between the pair of contacts and the *x*-axis (after [23]).

$InAs/Al_{0.3}Ga_{0.7}Sb$ single QW of 15 nm width at room temperature. Because of the admixture of photon handedness-independent magneto-gyrotropic effects (see subsection 5.2), the spin-galvanic effect is extracted after eliminating this current contribution: $j = (j_{\sigma_+} - j_{\sigma_-})/2$.

The nonequilibrium in-plane spin polarization $\boldsymbol{S}_\parallel$ is prepared as described in section 4 (see also figure 6(*a*)). The angle between the magnetic field and $\boldsymbol{S}_\parallel$ can in general depend on details of the spin relaxation process. In these particular InAs QW structures the isotropic Elliott–Yafet spin relaxation mechanism dominates. Thus, the in-plane spin polarization $\boldsymbol{S}_\parallel$ is always perpendicular to $\boldsymbol{B}$ and can be varied by rotating $\boldsymbol{B}$ around z as illustrated in figure 6(*a*). The circle in figure 6(*c*) represents the angular dependence $\cos(\vartheta - \vartheta_{\max})$, where ϑ is the angle between the pair of contacts and the *x*-axis and $\vartheta_{\max} = \arctan j_R/j_D$. The best fit in this sample is achieved for the ratio $j_R/j_D = \alpha/\beta = 2.1$. The method was also used for the investigation of Rashba/Dresselhaus spin splitting in GaAs/AlGaAs heterostructures [24] where the spin relaxation is controlled by the D'yakonov–Perel' mechanism. These experiments demonstrate that the growth of structures with various δ-doping layer positions accompanied by experiments on the spin-galvanic effect makes possible a controllable variation of the structural inversion asymmetry and preparation of samples with equal Rashba and Dresselhaus constants or with a zero Rashba constant.

The effect inverse to the spin-galvanic effect is the electron spin polarization generated by a charge current $\boldsymbol{j}$. It was predicted in [25] and observed in bulk tellurium [26]. It was further demonstrated that spin orientation by current is also possible in QW systems [27–29]. This study was extended in [30–35]. Most recently, the first direct experimental proofs of this effect were obtained in semiconductor QWs [36, 37] as well as in strained bulk material [38]. At present the inverse spin-galvanic effect has been observed in various low-dimensional structures based on GaAs, InAs, ZnSe and GaN applying various experimental techniques, comprising transmission of polarized THz radiation, polarized photoluminescence and space-resolved Faraday rotation [36–42].

In some structures, however, the helicity dependence of the photocurrent is not as simple as shown in figure 5, where the current is proportional to the radiation helicity. It has been observed that the dependence of the magneto-induced photocurrent can show beatings caused by interplay of two terms, one being $\propto \sin 2\varphi$ and the other $\propto \sin 4\varphi$. The latter term stems for the MGE due to zero-bias spin separation and in some structures can even play a dominant role overweighing the spin-galvanic effect. Such an interplay is shown in figure 7 for GaN/AlGaN heterojunction for the photocurrent measured along the magnetic field. Similar dependences have been observed in GaAs- and InAs-based QWs. The contribution $\propto \sin 4\varphi$ directly follows from the phenomenological theory (see equation (5)) and corresponds to the degree of linear polarization described by the Stokes parameter $P_{\rm lin} = \sin 4\varphi/4$. It can be investigated without admixture of the spin-galvanic effect applying linearly polarized radiation. In the next subsection we consider details of this type of magneto-gyrotropic effects.

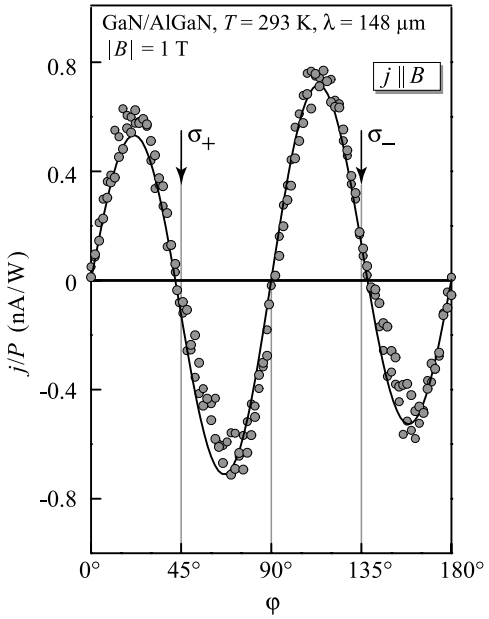

Figure 7. Magnetic-field-induced photocurrent J as a function of the phase angle φ defining the radiation helicity. The photocurrent signal is measured in GaN/AlGaN heterojunction at room temperature in the longitudinal geometry $\boldsymbol{j} \parallel \boldsymbol{B}$ under normal incidence of the radiation with $P \approx 10$ kW. The full line is the fit after the second equation of (9). After [43].

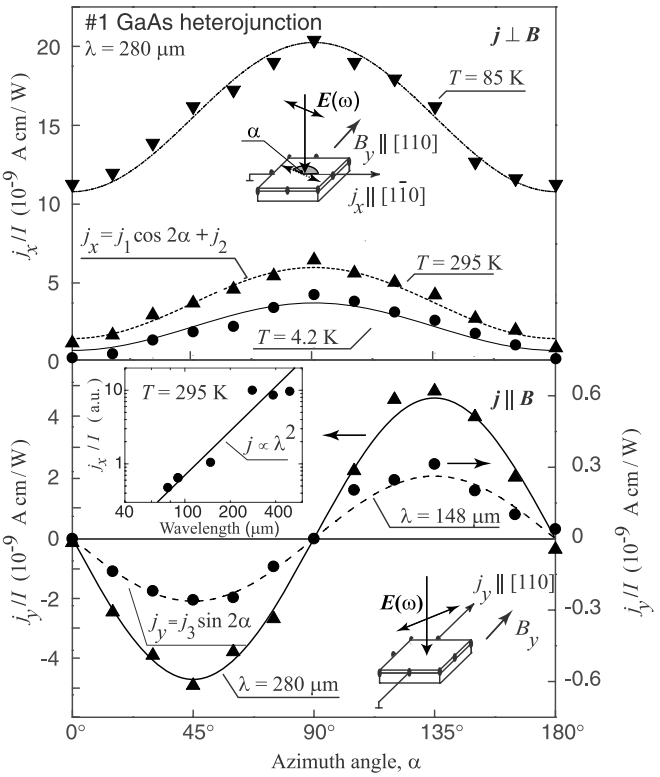

Figure 8. Photocurrents for GaAs/AlGaAs heterojunction as a function of angle α. Data are obtained at $B_y = 0.3$ T. Upper panel: photocurrent $\boldsymbol{j} \perp \boldsymbol{B} \| y$ at $\lambda = 280$ μm and T = 4.2 K, 85 K and 295 K. Lines are fits according to $j_x = j_1 \cos 2\alpha + j_2$. Lower panel: photocurrent $\boldsymbol{j} \| \boldsymbol{B} \| y$ measured at room temperature for $\lambda = 148$ and 280 μm. Lines are fitted to $j_y = j_3 \sin 2\alpha$. Insets show the experimental geometries. An additional inset in the lower panel displays the wavelength dependence of the signal for transverse geometry, the full line shows $j_x \propto \lambda^2$. From [12].

5.2. Magneto-gyrotropic effects due to the zero-bias spin separation

Magneto-gyrotropic effects due to the zero-bias spin separation do not require circularly polarized light and can be observed applying linearly polarized or even unpolarized radiation. As in the previous case of the spin-galvanic effect the current pulse follows the excitation pulse shape and its direction reverses upon the change of the magnetic field direction, however it does not depend on the radiation handedness. Figure 8 shows a typical variation of the photocurrent upon changes of the azimuth angle α for the in-plane magnetic field aligned along the y-axis, B_y. The data are obtained for (0 0 1)-grown GaAs/AlGaAs heterojunction at normal incidence with terahertz radiation resulting in the Drude-like absorption [12]. The polarization dependence of the current $\boldsymbol{j}$ is well described by the phenomenological equations (8) and correspondingly can be well fitted in the transverse geometry by $j_x = j_1 \cos 2\alpha + j_2$ and by $j_y = j_3 \sin 2\alpha$ for the longitudinal geometry. In the following, we will use the definitions $j_1 = S_2 B_y I$, $j_2 = S_1 B_y I$, $j_3 = S_3' B_y I$. We note that for the photocurrent detected in the direction perpendicular to the magnetic field a polarization independent offset is observed, demonstrating that this effect can appear for excitation with unpolarized radiation.

The variation of the photocurrent strength and direction upon changing of the azimuth angle is a characteristic of the MGE due to Drude absorption [13]. In this case the polarization dependences of the photocurrent remain the same, independent of temperature, wavelength and material. An increased wavelength at constant intensity results in an increased signal strength only. The wavelength dependence for both configurations is described by $j \propto \lambda^2$ for the wavelengths used (see the inset in figure 8, lower panel) and reflects the spectral behavior of Drude absorption, $\eta(\omega) \propto 1/\omega^2$ at $\omega\tau_p \gg 1$ (see [44]). Here $\eta(\omega)$ is the 2DEG's absorbance at the frequency ω. For intersubband transitions excited by the mid-infrared radiation MGE has also been observed. In this case, the photocurrent is detected in the direction perpendicular to the magnetic field only and does not show any polarization dependence. This result is not surprising because, in contrast to the Drude mechanism, absorption due to direct intersubband transitions does not rely on scattering and the photoexcitation mechanism of the photocurrent caused is absent.

The key experiment supporting microscopic mechanisms discussed in subsection 2.2 is the investigation of the temperature dependence of the photocurrent. The analysis shows [45] that for fixed polarization for both excitation and relaxation mechanisms (figures 3(*a*) and (*b*)) the current is proportional to the frequency-dependent absorbance $\eta(\omega)$, momentum relaxation time τ_p, light intensity I and average spin S: $j \propto \eta(\omega) I \tau_p S$. Such a type of expression for the temperature dependence is valid for fixed scattering mechanism, e.g., phonon or impurity scattering. For Drude absorption, the temperature dependence of the current can be reduced to $n_s S$. Since Drude absorption, $\eta(\omega) \propto n_s/\tau_p$ at $\omega\tau_p \gg 1$ (see [44]) and at low temperatures $S \propto 1/\varepsilon_F \propto 1/n_s$ (see equation (4)), the current $j/I \propto \tau_p \eta(\omega) S$ is constant and independent of τ_p and n_s. At high temperatures S is sufficiently well described by the Boltzmann distribution and hence $S \propto 1/k_B T$, see equation (4). Therefore, the current j is proportional to n_s/T and becomes temperature dependent, concordant with experiment. An example of such temperature behavior is shown in figure 9 where the temperature dependences of the currents j_1 and j_2 corresponding to the excitation and relaxation mechanisms are depicted. The data are obtained in an n-type SiGe QW structure for the magnetic field 0.6 T under excitation with radiation of $\lambda = 148$ μm wavelength.

The theory of the magneto-gyrotropic effect due to zero-bias spin separation caused by Drude absorption and relaxation of heated electron gas has been developed in [12]. Besides characteristic temperature and polarization dependences this theory demonstrates that the photocurrent is proportional to the degree of inversion asymmetry. This is a natural result because the asymmetry of scattering is due to BIA/SIA. The experiments carried out on samples with different degrees of asymmetry show that the current strength is indeed proportional to the degree of structural asymmetry. Moreover, the photocurrent reverses its direction upon reversing sign of the SIA contribution. This is demonstrated by figure 10 which shows j_1 and j_2 attributed to the photoexcitation (figure 3(*b*)) and to the relaxation

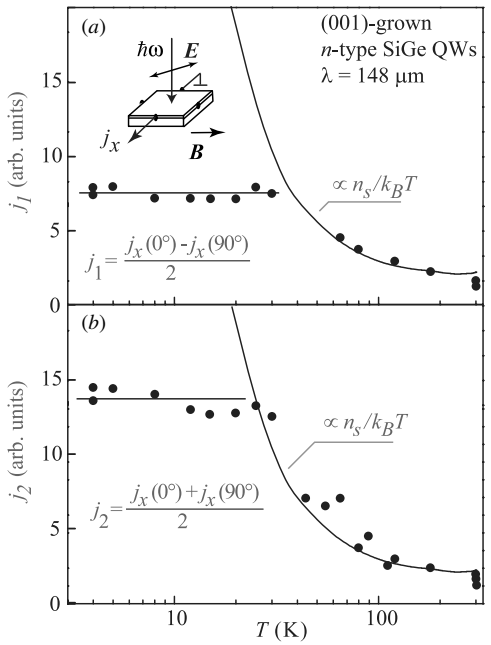

Figure 9. Temperature dependences of the contributions j_1 (*a*) and j_2 (*b*) to the photocurrent j_x in a magnetic field $\boldsymbol{B} \parallel y$ ($B = 0.6$ T). Full lines are fits to An_s/k_BT with a single fitting parameter A and to a constant. From [45].

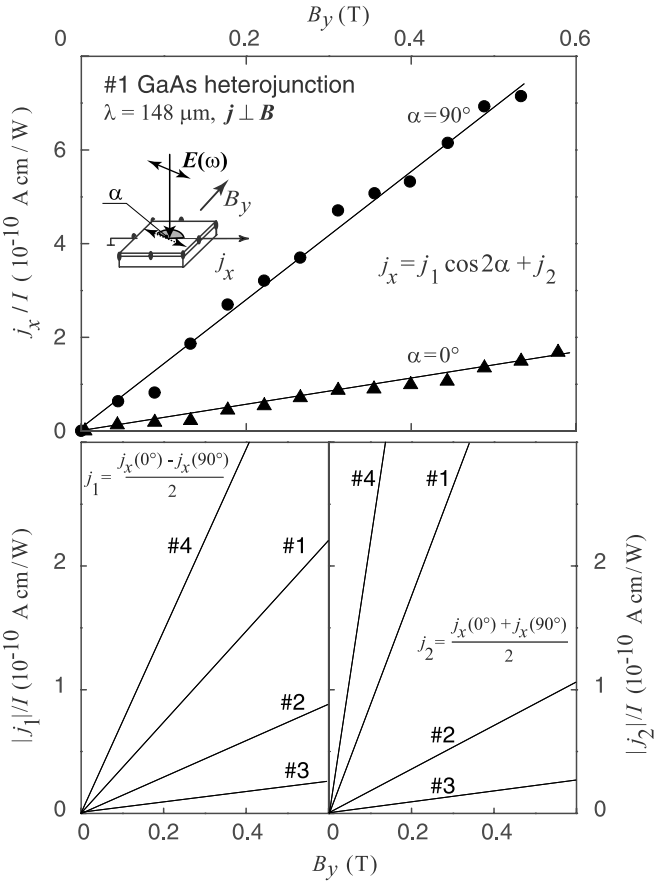

Figure 10. Magnetic field dependences of the transverse photocurrent. Upper panel: $j_x(B)$ normalized by radiation intensity I, measured for GaAs-based heterojunction (sample 1) at room temperature for $\alpha = 90°$ and $\alpha = 0°$. Lower panels: $j_1(B)$ (left panel) and $j_2(B)$ (right panel) obtained by subtracting and adding the currents for the two polarization directions for samples 1–4 (after [12]).

(figure 3(*a*)) mechanisms, respectively. Due to the larger *g*-factor of sample 4 (InAs QW), causing larger average spin S, the currents are largest for this structure. The other three samples are GaAs-based heterostructures which differ in structural inversion asymmetry. Sample 1 is a heterojunction which, due to the triangular confinement potential, is expected to have the strongest SIA contribution. Samples 2 and 3 are quantum wells of the same width, asymmetrically and symmetrically modulation doped, with larger and smaller strength of SIA, respectively. The fact that with decreasing strength of the SIA coupling coefficient (from sample 1 to 3) the currents become smaller in excellent agreement with our picture of asymmetric scattering-driven currents.

5.3. Magneto-gyrotropic effect in (1 1 0)-grown quantum wells

Most recently, magneto-gyrotropic effects have been applied to conclude on symmetry and spin dephasing in (1 1 0)-grown quantum wells. Quantum wells on (1 1 0)-oriented GaAs substrates attract growing attention in spintronics due to their extraordinary slow spin dephasing [46–49]. The reason for the long spin lifetime of several nanoseconds is the (1 1 0) crystal orientation: then the effective magnetic field due to spin–orbit coupling points into the growth direction [8] and spins oriented along this direction do not precess. Hence, the D'yakonov–Perel' spin relaxation mechanism [21] which is based on the spin precession in the effective magnetic field and usually limits the spin lifetime of conduction electrons is suppressed. If, however, QWs are asymmetric, the structural inversion symmetry is broken and Rashba spin–orbit coupling causes an in-plane effective magnetic field, thus speeding-up spin dephasing. To judge the symmetry of QWs, one has to rely on the growth process but no independent method to check the structure symmetry is readily available. The magneto-gyrotropic effect is an ideal tool to probe the symmetry of (1 1 0)-grown QWs. The photocurrent is only observed for asymmetric structures but vanishes if QWs are symmetric. This statement has also been supported by time-resolved Kerr rotation that the spin relaxation time is maximal in QW which does not show MGE.

In [50], the structural inversion asymmetry has been varied by the δ-doping position with respect to the QW. Quantum wells differ essentially in their doping profile: sample A is a single heterojunction and has the strongest asymmetry stemming from the triangular confinement potential. In samples B and D, the doping layers are asymmetrically shifted off the barrier center either to the left or to the right, respectively. This asymmetric doping yields an asymmetric potential profile inside the QWs. Samples grown along $z \parallel [1\,1\,0]$ were square shaped with the sample edges of 5 mm length oriented along $x \parallel [1\,\bar{1}\,0]$ and $y \parallel [0\,0\,\bar{1}]$. The degree of SIA is reflected in the magnetic field dependence of the photocurrent displayed in figure 11. The currents shown

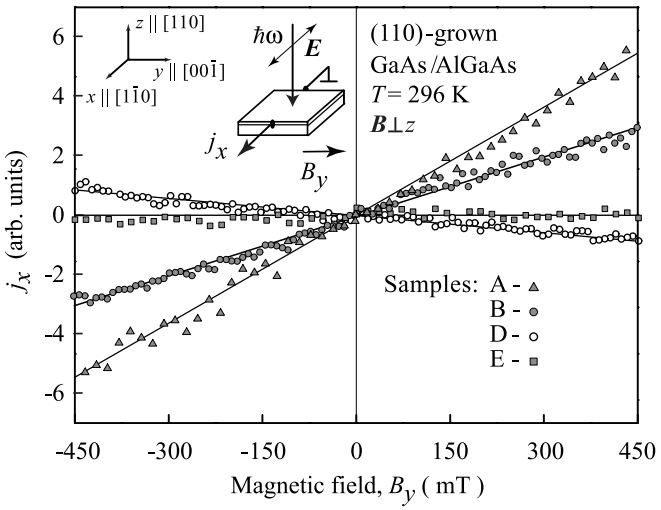

Figure 11. Magnetic field dependences of j_x for the radiation polarized along the x-axis and an in-plane magnetic field, $\boldsymbol{B} \parallel y$ (after [50]).

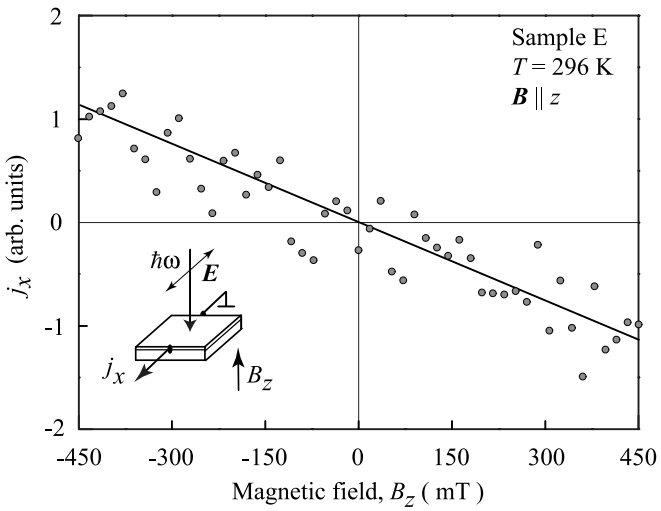

Figure 12. Magnetic field dependence of j_x for the radiation polarized along the x-axis and an in-plane magnetic field normal to the QWs, $\boldsymbol{B} \parallel z$ (after [50]).

in this figure are directly proportional to the applied field but the slope of $j_x(B_y)$ is sample dependent. The largest slope is obtained for sample A with the strongest asymmetry while the slope vanishes for the symmetric sample E. In the case of sample D, having opposite SIA, the slope is also negative.

We consider MGE induced by radiation polarized along the x-axis, as used in this experiment. For this geometry, the MGE current $j_x = \sum_\beta \phi_{x\beta xx} B_\beta |E_x|^2$ is phenomenologically determined by the coupling of the x-component of the current polar vector with the axial vector of the magnetic field, because $|E_x|^2$ is an invariant in (1 1 0)-grown structure. Therefore, the photocurrent can occur only for certain $\boldsymbol{B}$-components which are transformed equally to j_x for all symmetry operations. While the symmetry of perfectly symmetric (1 1 0)-grown QWs belong to the point group C_{2v}, asymmetric QWs belong to the point group C_s. The point group C_s contains only two symmetry elements: identity and a mirror plane m_1, perpendicular to the x-axis. For C_s group symmetry requirements are fulfilled for j_x and B_y or B_z only. Indeed, reflection by the m_1-plane reverses the sign of j_x ($j_x \to -j_x$) and two components of the magnetic field $\boldsymbol{B}$ ($B_y \to -B_y$ and $B_z \to -B_z$). Thus, the MGE can occur for magnetic fields aligned in-plane and out-of-plane of the QW and the photocurrent is given by

$$j_x^{C_s} = \phi_{xyxx}^{\mathrm{SIA}} B_y |E_x|^2 + \phi_{xzxx}^{\mathrm{BIA}} B_z |E_x|^2 \qquad (13)$$

with tensor components $\phi_{xyxx}^{\mathrm{SIA}}$ and $\phi_{xzxx}^{\mathrm{BIA}}$ determined by the degree of the SIA and BIA, respectively. If the magnetic field is applied in the y-direction, the last term in equation (13) becomes zero and the MGE current is determined solely by the degree of SIA.

The experiment displayed in figure 11 shows that the magnitude of the $j(B_y)$-slope strongly depends on the doping profile. Furthermore, if the doping profile is reversed (from samples B to D), the slope of the photocurrent gets reversed too (see figure 11). As the MGE current is proportional to the SIA coefficient, these observations demonstrate that the position of the doping layer can be effectively used for tuning the structure asymmetry strength. In particular, the sign of $\phi_{xyxx}^{\mathrm{SIA}}$ can be inverted by putting the doping layer on the other side of the QW.

While for an in-plane magnetic field the photogalvanic effect, described by equation (13), is observable in asymmetrical structures, it is forbidden in symmetrically grown QWs with the higher point group symmetry C_{2v}. This is caused by the presence of an additional mirror plane, m_2, being parallel to the QW plane of symmetrically grown (1 1 0)-structures. Indeed, reflection by this plane does not modify j_x but changes the polarity of the in-plane axial vector $\boldsymbol{B}$. Therefore, in such systems linear coupling of j_x and B_y is forbidden. On the other hand, mirror reflection of plane m_2 does not modify the z-component of $\boldsymbol{B}$. Thus the coupling of j_x and B_z is allowed for reflections by both m_1 and m_2 planes, and photocurrent j_x can occur in symmetric (1 1 0)-oriented QWs in the presence of a magnetic field in the z-direction. For this symmetry, equation (5) is reduced to

$$j_x^{C_{2v}} = \phi_{xzxx}^{\mathrm{BIA}} B_z |E_x|^2. \qquad (14)$$

This equation fully describes the data taken from sample E obtained for the in-plane magnetic field (figure 11) and the out-of-plane magnetic field (figure 12). There no MGE is observed for the in-plane magnetic field but a sizeable effect is detected for $\boldsymbol{B}$ applied normal to the QW plane. In the case of sample E, the absence of a magnetic-field-induced photocurrent in an in-plane $\boldsymbol{B}$ indicates that the QW is highly symmetric and lacks the structure asymmetry. The signal observed in the same structure for an out-of-plane B_z-field stems from the BIA term (see equation (14)). Hence, measurement of the MGE gives us an experimental handle to analyze the degree of SIA.

The structural inversion asymmetry determines the Rashba spin splitting and therefore controls the D'yakonov–Perel' relaxation [21] for spins aligned along the z-direction. Any variation of SIA, e.g., due to asymmetric doping, should result in a variation of the spin relaxation time. To directly

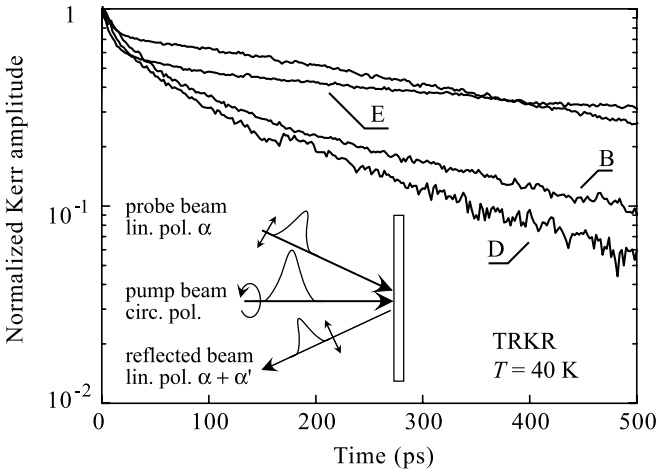

Figure 13. Kerr rotation measured in asymmetrically grown QWs samples B, D and symmetrical structure E. We note that the fast decaying components in the TRKR signals at short times are due to spin relaxation of photoexcited holes (after [50]).

demonstrate this connection, we compare spin relaxation rates measured in the symmetrically doped QW sample E and the asymmetrically doped QW samples B and D (figure 13). We extract the spin lifetime τ_s from time-resolved Kerr rotation (TRKR) measurements. The time evolution of the Kerr rotation angle tracks the spin polarization within the sample. By fitting an exponential decay function to the data, τ_s is determined. In correspondence to the above photocurrent measurements, indicating a larger degree of asymmetry of samples B and D compared to E, τ_s in sample E is found to be more than three times larger than that in sample B and about two times larger than in sample D.

Acknowledgments

We thank E L Ivchenko, L E Golub and S A Tarasenko for helpful discussions. This work is supported by the DFG and RFBR.

References

[1] Meier F and Zakharchenya B P (ed) 1984 *Optical Orientation (Modern Problems in Condensed Matter Sciences* vol 8*)* ed V M Agranovich and A A Maradudin (Amsterdam: Elsevier)
[2] D'yakonov M I and Perel' V I 1971 *Sov. JETP Lett.* **13** 144
[3] Averkiev N S and D'yakonov M I 1983 *Sov. Phys.—Semicond.* **17** 393
[4] Bakun A A, Zakharchenya B P, Rogachev A A, Tkachuk M N and Fleisher V G 1984 *Sov. JETP Lett.* **40** 1293
[5] Ganichev S D and Prettl W 2006 *Intense Terahertz Excitation of Semiconductors* (Oxford: Oxford University Press)
[6] Ivchenko E L, Lyanda-Geller Yu B and Pikus G E 1989 *JETP Lett.* **50** 175
[7] Ganichev S D *et al* 2002 *Nature* **417** 153
[8] D'yakonov M I and Kachorovskii V Yu 1986 *Sov. Phys.—Semicond.* **20** 110
[9] Bychkov Yu A and Rashba E I 1984 *JETP Lett.* **39** 78
[10] Averkiev N S, Golub L E and Willander M 2002 *J. Phys.: Condens. Matter* **14** R271
[11] Ivchenko E L and Pikus G E 1983 *Bull. Acad. Sci. USSR Phys. Ser.* **47** 81
[12] Ganichev S D *et al* 2006 *Nature Phys.* **2** 609
[13] Bel'kov V V *et al* 2005 *J. Phys.: Condens. Matter* **17** 3405
[14] Ganichev S D *et al* 2003 *Phys. Rev.* B **68** 081302
[15] Ivchenko E L 2005 *Optical Spectroscopy of Semiconductor Nanostructures* (Harrow: Alpha Science Int.)
[16] Ganichev S D and Prettl W 2003 *J. Phys.: Condens. Matter* **15** R935
[17] Ganichev S D *et al* 2003 *J. Supercond.: Incorporating Novel Magn.* **16** 369
[18] Tarasenko S A *et al* 2003 *J. Supercond.: Incorporating Novel Magn.* **16** 419
[19] Ivchenko E L and Tarasenko S A 2004 *JETP* **99** 379
[20] Golub L E 2007 *JETP Lett.* **85** 393
[21] D'yakonov M I and Perel' V I 1971 *Sov. Phys.—Solid State* **13** 3023
[22] Ivchenko E L 2002 private communication
[23] Ganichev S D *et al* 2004 *Phys. Rev. Lett.* **92** 256601
[24] Giglberger S *et al* 2007 *Phys. Rev.* B **75** 035327
[25] Ivchenko E L and Pikus G E 1978 *JETP Lett.* **27** 604
[26] Vorob'ev L E *et al* 1979 *JETP Lett.* **29** 441
[27] Aronov A G and Lyanda-Geller Yu B 1989 *JETP Lett.* **50** 431
[28] Edelstein V M 1990 *Solid State Commun.* **73** 233
[29] Vasko F T and Prima N A 1979 *Sov. Phys.—Solid State* **21** 994
[30] Aronov A G, Lyanda-Geller Yu B and Pikus G E 1991 *Sov. Phys.—JETP* **73** 537
[31] Chaplik A V, Entin M V and Magarill L I 2002 *Physica* E **13** 744
[32] Vasko F T and Raichev O E 2005 *Quantum Kinetic Theory and Applications* (New York: Springer)
[33] Tarasenko S A 2006 *JETP Lett.* **84** 199
[34] Trushin M and Schliemann J 2007 *Phys. Rev.* B **75** 155323
[35] Raichev O E 2007 *Phys. Rev.* B **75** 205340
[36] Ganichev S D *et al* 2004 *Preprint* See also Ganichev S D *et al* 2006 *J. Magn. Magn. Mater.* **300** 127
[37] Silov A Yu *et al* 2004 *Appl. Phys. Lett.* **85** 5929
[38] Kato Y K, Myers R C, Gossard A C and Awschalom D D 2004 *Phys. Rev. Lett.* **93** 176601
[39] Silov A Yu *et al* 2005 *Proc. 13th Int. Symp. Nanostructures: Phys. and Technol. (St Petersburg, Russia)*
[40] Sih V *et al* 2005 *Nature Phys.* **1** 31
[41] Stern N P *et al* 2006 *Phys. Rev. Lett.* **97** 126603
[42] Yang C L *et al* 2006 *Phys. Rev. Lett.* **96** 186605
[43] Weber W *et al* 2008 *Solid State Commun.* **145** 56
[44] Seeger K 2004 *Semiconductor Physics: An Introduction* (Berlin: Springer)
[45] Ganichev S D *et al* 2007 *Phys. Rev.* B **75** 155317
[46] Ohno Y *et al* 1999 *Phys. Rev. Lett.* **83** 4196
[47] Karimov O Z *et al* 2003 *Phys. Rev. Lett.* **91** 246601
[48] Döhrmann S *et al* 2004 *Phys. Rev. Lett.* **93** 147405
[49] Hall K C *et al* 2005 *Appl. Phys. Lett.* **86** 202114
[50] Bel'kov V V *et al* 2008 *Phys. Rev. Lett.* **100** 176806